

# Photoinduced quasiparticle dynamics of single CuO<sub>2</sub>-layer Bi-based cuprates with out-of-plane disorder

T. Akiba, Y. Toda , and S. Tsuchiya 


*Department of Applied Physics, Hokkaido University, Sapporo 060-8628, Japan*

M. Oda

*Department of Physics, Hokkaido University, Sapporo 060-0810, Japan*

T. Kurosawa

*Department of Applied Sciences, Muroran Institute of Technology, Muroran 050-8585, Japan*

D. Mihailovic and T. Mertelj 

*Complex Matter Department, Jozef Stefan Institute, Jamova 39, Ljubljana, SI-1000, Slovenia*



(Received 21 August 2023; accepted 18 December 2023; published 9 January 2024)

Optimally-doped (OPD) Bi<sub>2</sub>Sr<sub>1.7</sub>R<sub>0.3</sub>CuO<sub>6+δ</sub> (*R*-Bi2201, *R* = Eu and La) are investigated from the viewpoint of photoinduced nonequilibrium quasiparticle dynamics of high-*T<sub>c</sub>* cuprates with low *T<sub>c</sub>*. The temperature dependencies of the superconducting (SC) and pseudogap (PG) responses demonstrate that the out-of-plane disorder enhanced by replacing La with Eu reduces the SC transition temperature and increases the PG energy. SC fluctuations are observed in each sample, especially in *R* = La, where large SC fluctuations, which deeply penetrate into the PG state, are observed. From the fluence-dependent dynamics, the planar optical destruction energy densities of the SC state are found consistent with the *T<sub>c</sub>*<sup>2</sup> dependence noted previously for other high-*T<sub>c</sub>* superconductors. Upon an optical quench we find that the SC state recovery starts only after the completion of the PG recovery in both samples.

DOI: [10.1103/PhysRevB.109.014503](https://doi.org/10.1103/PhysRevB.109.014503)

## I. INTRODUCTION

The pseudogap (PG) observed in the cuprate high-*T<sub>c</sub>* superconductors (SCs) has long been studied using various techniques as a key to elucidate the mechanism of high-*T<sub>c</sub>* superconductivity [1]. As a widely accepted finding, angle-resolved photoemission spectroscopy (ARPES) has revealed that Fermi surfaces with *d*-wave gaps can be divided into nodal regions, mainly involved in the SC gap, and antinodal regions, reflecting the PG, and that these two energy gaps compete in *k* space [2–4]. The presence of symmetry breaking is another characteristic PG feature [5], where the charge ordering has been visualized in real space by tunneling spectroscopy (STM/STS) [6,7]. Recent STM studies reveal that the charge order is positively correlated to the periodic modulation of the Cooper pair density [8]. Moreover, nematic ordering and loop current ordering have been observed, for example, by magnetic torque measurements [9] and polarized neutron-scattering measurements [10]. The second-order nematic transition implies the existence of a quantum critical point in the SC dome, where the quantum fluctuation properties should also affect the SC.

The study of out-of-plane disorder is important because it is closely related to the maximum *T<sub>c</sub>* [11–15] and the Fermi surface properties [16], where the PG appears suppressed already at low doping in extremely clean CuO<sub>2</sub> planes. Recent nuclear magnetic resonance (NMR) studies report that

when external pressure is applied that promotes higher *T<sub>c</sub>*, the pressure leads to a redistribution of holes in favor of the oxygen plane [17]. The in-plane oxygen orbitals are known to play an important role in density-wave ordering in the PG state [18]. In fact, ARPES experiments have reported that the enhanced out-of-plane disorder reduces the *T<sub>c</sub>*, but develops the antinodal PG, while the superconducting gap dispersion around the nodes remains almost unchanged [19,20].

Photoinduced nonequilibrium techniques using femtosecond laser pulse excitation are another attractive way to study the SC and PG properties and their dynamics that cannot be assessed by steady state measurements [21]. In particular, the quasiparticle excitation at the PG is accompanied by spectral changes that extend into the near-infrared region formed by electron correlations, and thus all-optical time-resolved spectroscopy is highly sensitive to the PG [22,23]. Indeed, the PG response with sub-picosecond (ps) relaxation has been universally observed in a variety of high-*T<sub>c</sub>* cuprates, and the doping dependence of the gap values are in good agreement with those determined by other low-energy spectroscopy measurements [24–29]. In contrast to the fast PG response, the SC response, attributed to the quasiparticle relaxation across the SC gap, displays longer relaxation times, on the picoseconds timescale. These two components can therefore be identified based on the relaxation time difference between them.

Rotational symmetry breaking associated with nematic order has also been observed as an anisotropic polarization

dynamics synchronized with the onset of the PG [30,31]. On the other hand, optical quench dynamics of the PG has shown no critical relaxation expected for a long-range order [32].

In this study, ultrafast optical time-resolved measurements are performed on optimally-doped (OPD)  $\text{Bi}_2\text{Sr}_2\text{CuO}_{6+\delta}$  (Bi2201). The single- $\text{CuO}_2$ -plane OPD-Bi2201 shows a lower maximum  $T_c$  than Bi2212, allowing for a larger energy difference between the SC gap and PG, which is useful for time-resolved analysis of multiple response components. Although some photoinduced nonequilibrium studies of Bi2201 provided important insights into the Mott physics [33] and electron-boson interaction [34], the SC and PG response properties and their correlation have not been clarified.

In particular, we present the photoinduced nonequilibrium properties of  $\text{Bi}_2\text{Sr}_{1.7}\text{R}_{0.3}\text{CuO}_{6+\delta}$  ( $R$ -Bi2201) with two different rare-earth ( $R$ ) substitutions, where  $R$  induces disorder to the  $\text{CuO}_2$  conduction plane, the magnitude of which increases for  $R = \text{Eu}$  compared to the case of  $R = \text{La}$  [19,20,35,36].

The relaxation time of the SC response of  $R$ -Bi2201 reaches the order of 10 ps, more than twice longer than that of Bi2212. In contrast, the relaxation time of the PG response is less than 1 ps, comparable to that of Bi2212. Using these characteristics, we perform time-selective analysis for the temperature and fluence dependencies of the transient reflectivity,  $\Delta r/r$ , and verify that the out-of-plane disorder enhanced by replacing  $R = \text{La}$  with  $R = \text{Eu}$  increases the PG energy and reduces  $T_c$ . The presence of the SC fluctuations is confirmed in both samples, and especially in  $R = \text{La}$ , where the fluctuations appear at temperatures more than 10 K higher than  $T_c$ . The 3-pulse quench spectroscopy indicates that the start of the SC state recovery and the completion of PG state recovery are synchronous in each sample.

## II. EXPERIMENTAL

Single crystals of rare-earth substituted  $\text{Bi}_2\text{Sr}_{1.7}\text{R}_{0.3}\text{CuO}_{6+\delta}$  ( $R$ -Bi2201) were grown in 1 atm of flowing oxygen with  $R = \text{La}$  and  $\text{Eu}$  content of 0.3, corresponding to optimal doping levels as reported previously [12,36]. Two samples, La-Bi2201 ( $T_c^m = 34$  K) and Eu-Bi2201 ( $T_c^m = 20$  K), were measured, where  $T_c^m$ 's were evaluated from the magnetic susceptibility measurements (see Fig. 8 in Appendix A).

The freshly-cleaved samples were mounted in a He-flow cryostat with optical windows. The time evolution of the photoinduced transient reflectivity  $\Delta r/r$  was monitored using a conventional pump (P-pulse; 400 nm, 3.1 eV), and probe (pr-pulse; 800 nm, 1.55 eV) spectroscopy. The recovery dynamics of SC and PG states were also measured using the 3-pulse optical quench spectroscopy, which combines the standard pump-probe spectroscopy with a destruction pulse (D pulse; 400 nm, 3.1 eV) that can destroy the SC and PG states in the photoexcited region.

All pulses were linearly polarized and derived from a cavity-dumped mode-locked Ti: sapphire laser with the pulse duration of approximately 120 fs, the central wavelength of 800 nm and the repetition rate of 270 kHz. The second harmonic of the laser is used for the P and D pulses. All pulses were coaxially combined and focused onto the sample using an objective lens. The polarization of the P pulse was set

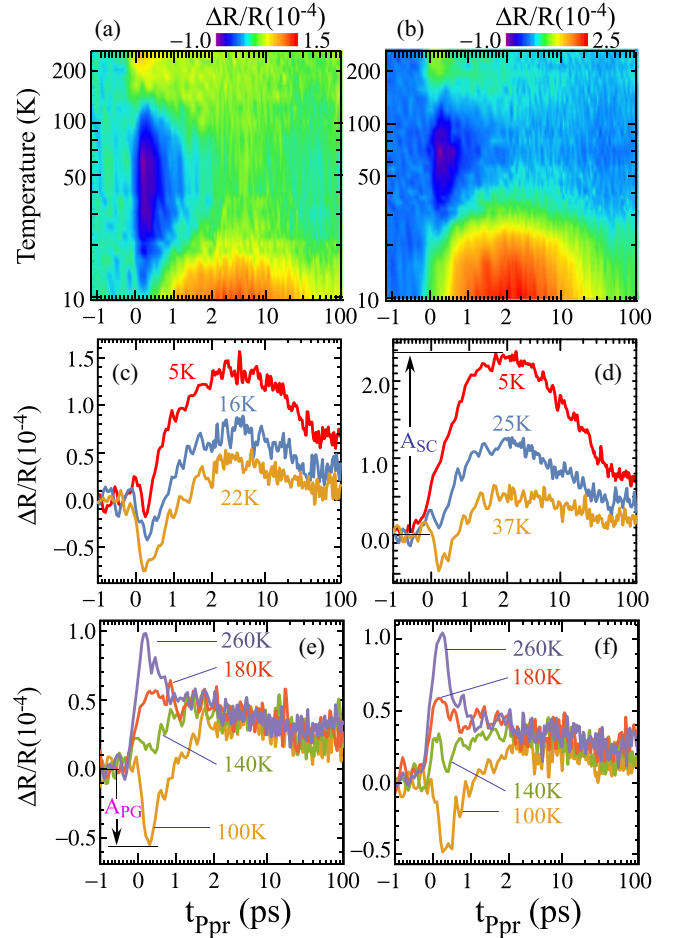


FIG. 1. The temperature dependencies of  $\Delta r/r$  for (left) Eu-Bi2201 and (right) La-Bi2201 with the pump fluence of  $\mathcal{F}_p = 45 \mu\text{J}/\text{cm}^2$ . [(a), (b)] Color plots of  $\Delta r/r$  as functions of delay time (horizontal axis,  $t_{\text{ppr}}$ ) and the log of temperature (vertical axis). [(c), (d)] Typical  $\Delta r/r$  in the temperature range below around  $T_c$ . [(e), (f)] Typical  $\Delta r/r$  in the temperature range well above  $T_c$ .

parallel to the pr pulse and the polarization of the D pulse was set perpendicular ( $\mathbf{E}_p \parallel \mathbf{E}_{\text{pr}} \perp \mathbf{E}_D$ ). The spot sizes are estimated to be  $25 \times 13 \mu\text{m}^2$  for P and D pulses,  $36 \times 23 \mu\text{m}^2$  for 2-pulse probe and  $10 \times 10 \mu\text{m}^2$  for 3-pulse pr pulse. The transient reflectivity of the pr-pulse was measured using a standard lock-in technique synchronized with the chopping frequency (280 Hz) of the P pulse. In the 3-pulse optical quench spectroscopy, we use the chopping of the pump to detect only the P-pulse-induced quasiparticle dynamics in the transient state after the D-pulse excitation.

## III. RESULTS

### A. Temperature dependence

The temperature ( $T$ ) dependencies of  $\Delta r/r$ , associated with quasiparticle dynamics [21], measured by the 2-pulse pump-probe spectroscopy in Eu-Bi2201 (left) and La-Bi2201 (right) are summarized in Fig. 1. The upper panels [Figs. 1(a) and 1(b)] are density plots of the transient reflectivity  $\Delta r/r$  where the vertical axis is the logarithm of the temperature. The slow decay component (warm color) that dominates in

the low-temperature region below  $T_c$  is attributed to the SC response, and the fast decay component (cold color) that remains above  $T_c$  is attributed to the PG response. Comparing the SC response (warm color) between Figs. 1(a) and 1(b), we see an increase in the onset temperature of the SC response reflecting the increase in the  $T_c$  associated with the decrease in the ionic radius of the substituted rare earth ions from Eu to La.

The transient responses observed at representative temperatures from the lowest temperature to the temperature just above  $T_c$  are shown in Figs. 1(c) and 1(d). The slow decay component, reflecting pairing recombination of the SC quasiparticles, is dominant in  $\Delta r/r$ . As the temperature increases across  $T_c$ , the SC response disappears and instead the PG response, which is characterized by the fast decay and opposite sign to the SC response, becomes dominant. As suggested by the density plots in Fig. 1, the PG response is present also below  $T_c$ , and contributes to the rise dynamics of  $\Delta r/r$ . The typical transient responses at representative temperatures in the range from  $T_c$  to room temperature are shown in Figs. 1(e) and 1(f).  $\Delta r/r$  at  $T = 260$  K corresponds to the metallic electron-phonon relaxation (EPR), which consists of a fast decay component with a relaxation slightly slower than the pulse width of the laser and a long decay component on the order of nanoseconds. The distinct PG response, observed in the vicinity of  $T_c$  gradually diminishes with increasing temperature and vanishes into the EPR response above  $T \sim 200$  K.

The combination of the above three transient response components is commonly observed in various high- $T_c$  cuprates by time-resolved spectroscopy with optical pulse excitation [21,24–30]. Here, we shortly summarize the characteristics of the  $R$ -Bi2201 by comparing to other high- $T_c$  cuprates. The SC response show a moderate increase with decreasing  $T$ ,  $\tau_{2p}^{SC} = 15$ –25 ps (at  $T = 20$ –5 K) in  $R = \text{Eu}$  and 10–15 ps (at  $T = 30$ –5 K) in  $R = \text{La}$ , which are more than two times slower than that of Bi2212 [30] and close to that of LSCO [27]. The slow decay time reflects the small SC gap that enhances the phonon bottleneck and thus increases the relaxation time across the gap. This is also consistent with the difference in  $\tau_{2p}^{SC}$  between  $R = \text{Eu}$  and  $R = \text{La}$  samples. In contrast, the relaxation time of  $\Delta r/r$  in the PG state is  $\sim 0.8$  ps, which is almost identical to that observed in Bi2212 and LSCO.

Below  $T_c$  [Figs. 1(c) and 1(d)], the delay times at which  $\Delta r/r$  shows a maximum value are about 5 ps for the  $R = \text{Eu}$  and about 2 ps for the  $R = \text{La}$ , where the contribution of the PG response can be neglected. We define this  $\Delta r/r$  as the SC response amplitude  $A_{SC}$  [the arrow on the left side of Fig. 1(d)], and its temperature dependence is shown in Fig. 2(a). Here the solid and open circles represent the data of Eu-Bi2201 and La-Bi2201, respectively. Note that we used the peak value of the SC response at a fixed delay as the definition with the least arbitrary elements. Similar results were obtained with a fitting procedure consisting of two components (SC and PG components) as described in Appendix B.

The  $T$  dependence of  $A_{SC}$  below  $T_c$  can be fairly fit by Mattis-Bardeen (MB) formula [37] [solid line in Fig. 2(a)] indicating that the SC state is completely suppressed at the particular pump fluence,  $\mathcal{F}_{pr}$ , as confirmed also from the fluence dependence discussed below in Sec. III B. The obtained

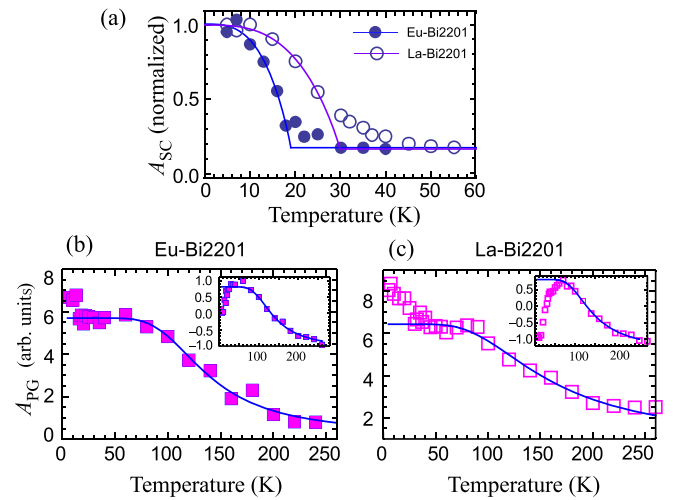


FIG. 2. (a) The temperature dependencies of the SC amplitudes  $A_{SC}$ , obtained by method (i), for (solid circles) Eu-Bi2201 and (open circles) La-Bi2201. The solid lines are fits to the data using the Mattis-Bardeen formula [39] with BCS-like gap function resulting in  $T_c = 19 \pm 0.6$  K for Eu-Bi2201 and  $30 \pm 1.6$  K for La-Bi2201. The residual component above  $T_c$  is attributed to the SC fluctuations while the high- $T$  offset is due to the EPR background. The temperature dependencies of the PG amplitudes  $A_{PG}$ , obtained by method (ii), for (b) Eu-Bi2201 and (c) La-Bi2201. The solid line in each graph is the fit to the data using Kabanov formula [40] based on the temperature independent gap. The inset in each plot shows  $A_{PG}$ , obtained by method (i), and the corresponding Kabanov formula fit. Note that in method (i)  $A_{PG}$  is defined with a minus sign,  $A_{PG} = -\Delta r/r|_{t_{pr}=300 \text{ fs}}$ .

$T_c = 19 \pm 0.6$  K ( $R = \text{Eu}$ ) and  $T_c = 30 \pm 1.6$  K ( $R = \text{La}$ ) are in good agreement with those obtained from magnetic susceptibility ( $T_c^m = 20$  K for  $R = \text{Eu}$  and  $T_c^m = 34$  K for  $R = \text{La}$ ). Within  $\sim 10$  K above  $T_c$   $A_{SC}$  significantly departs from the background (and the MB fit). The presence of the SC component at temperatures above  $T_c$  is attributed to the SC fluctuations [38].

As shown in Fig. 1, the PG response appears as a sharp negative peak in the time range  $t_{pr} = 0.2$ –0.5 ps and its decay time is almost temperature independent ( $\tau_{2p}^{PG} \approx 0.8$ –1 ps). In the temperature range of  $T > 75$  K, the amplitude of the PG response decreases with increasing temperature, but its presence can be identified as a dip in the EPR response [Figs. 1(e) and 1(f)]. The PG response thus overlaps with the EPR response in the normal state and the SC response below  $T_c$ .

In Bi2212 it was shown [32,41] that the EPR response is virtually  $T$  independent. The temperature evolution of  $\Delta r/r$  in the present case suggests the same behavior. The high- $T$   $\Delta r/r$  maximum appears at  $t_{pr} \sim 0.15$  ps while the  $\Delta r/r$  minimum in the PG state is delayed at  $t_{pr} = 0.3$  ps while at intermediate  $T$  both peaks are present simultaneously in the data. Moreover, as shown in Appendix B, subtraction of the high- $T$   $\Delta r/r$  from the lower- $T$  transients results in a single-exponential dynamics of the residual  $\Delta r_s/r$  in the PG state and two-component behavior in the SC state. We therefore analyze the data assuming that the highest- $T$   $\Delta r/r$  corresponds to the  $T$ -independent hot-electron [42] EPR response [32]. The



total  $\Delta r/r$  therefore consists of the EPR and PG components, which contribute mainly to the sub-picosecond response, and the slower SC component discussed above.

Due to similar timescales of the EPR, PG components and the SC risetime dynamics in combination to relatively small signal/noise ratio it is not possible to decompose the signal by multicomponent fitting. We therefore analyze the  $T$ -dependent data in two ways: (i) by a direct readout of  $\Delta r/r$  at the selected  $t_{\text{ppr}}$ 's, that maximize either the PG or SC component contribution and (ii) by two component fitting of the  $\Delta r_s/r$  presented in Appendix B. Both approaches give equivalent results.

In Figs. 2(b) and 2(c), we plot  $A_{\text{PG}}$  obtained by method (ii) and as inset by method (i) [43]. The solid lines are approximations of the temperature dependence of photoexcited carrier density using a temperature-independent gap  $\Delta_{\text{PG}}$  model derived by Kabanov *et al.* [40]. Considering that the SC fluctuations are present just above  $T_c$ , we omit fitting the model to the data in the temperature range below 50 K for  $R = \text{La}$  and below 30 K for  $R = \text{Eu}$ , respectively. The magnitudes of the PG estimated from the approximation are  $\Delta_{\text{PG}}^{\text{Eu}} = 54 \pm 5$  ( $48 \pm 4$ ) meV and  $\Delta_{\text{PG}}^{\text{La}} = 45 \pm 5$  ( $44 \pm 6$ ) meV [44]. The values in parentheses correspond to method (i), suggesting that the PG increases with increasing spatial inhomogeneity. The results also indicate the anticorrelated changes of the SC and PG gap with respect to the  $R$  substitution, which correspond well with the results of the previous ARPES and STM measurements [19,20,36].

By virtue of the low  $T_c$  of Eu-Bi2201, a temperature dependence is visible in the temperature range of  $T = 20$ –60 K, indicating a small contribution of thermally excited carriers across  $\Delta_{\text{PG}}$ . Note that the increase/decrease in the  $A_{\text{PG}}$  in the SC state has virtually identical shape to  $A_{\text{SC}}$ , and is due to the contribution of the SC component to  $A_{\text{PG}}$ , which has different sign depending on the method. As temperature increases, the number of photoexcited carriers decreases exponentially during the bottleneck because the photoexcitation energy is efficiently dissipated in phonon excitations [40]. This trend is consistent with the results for various high- $T_c$  cuprates [24–27,41,45]. On the other hand, the narrower flat temperature region in La-Bi2201 indicates that the SC fluctuations above  $T_c$  extend up to a larger  $T$ .

## B. Photoexcitation fluence dependence

The pump-fluence dependencies of the photo-induced quasiparticle dynamics measured by the 2-pulse pump-probe spectroscopy are summarized in Fig. 3 (left for  $R = \text{Eu}$  and right for  $R = \text{La}$ ). The  $\Delta r/r$  at the lowest temperature  $T = 10$  K, where the SC response dominates, are shown in Figs. 3(a) and 3(b), while  $\Delta r/r$  at  $T = 50$  K, where the PG response dominates, are shown in Figs. 3(c) and 3(d). Figures 3(e)–3(h) show plots of the SC and PG amplitudes as a function of the pump-fluence obtained by method (i) [46]. The high- $T$  measurements indicate a linear scaling of the EPR response with increasing fluence. However, method (ii) is very demanding experimentally since it would require high- $T$  fluence dependence measurements of the EPR component at identical conditions. The saturation regions deviating from

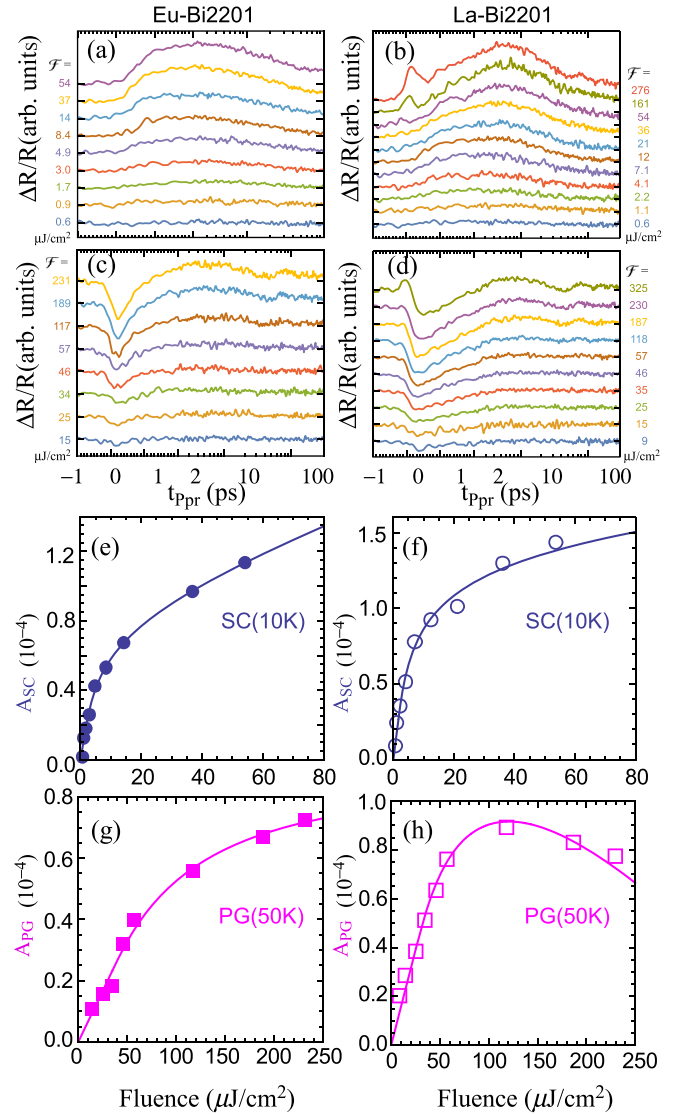


FIG. 3. The fluence dependencies for (left) Eu-Bi2201 and (right) La-Bi2201.  $\Delta r/r$  at various pump fluence [(a), (b)] at  $T = 10$  K and [(c), (d)] at 50 K. Each plot is vertically shifted for clarity. Plots of the SC [(e), (f)] and PG [(g), (h)] amplitudes derived from (a)–(d). The solid lines are the results of fitting by the analytical model given by Eq. (C3) [47], with estimated destruction thresholds of  $\mathcal{F}_{\text{th}}^{\text{SC}} = 1.4 \pm 0.4 \mu\text{J}/\text{cm}^2$  and  $\mathcal{F}_{\text{th}}^{\text{PG}} = 35 \pm 8 \mu\text{J}/\text{cm}^2$  for  $R = \text{Eu}$ , and  $\mathcal{F}_{\text{th}}^{\text{SC}} = 0.99 \pm 0.17 \mu\text{J}/\text{cm}^2$  and  $\mathcal{F}_{\text{th}}^{\text{PG}} = 25 \pm 3 \mu\text{J}/\text{cm}^2$  for  $R = \text{La}$ , respectively.

the linear dependence imply photoinduced phase destructions [47,48].

At small pump fluences [49], the transient response exhibits a linear scaling with the fluence [47], whereas as the fluence increases to the condition that induces a phase destruction in the photoexcited volume, the response deviates from the linear dependence. The saturation threshold  $\mathcal{F}_{\text{th}}^{\text{SC}}$  is derived from the fit to the data using the model that takes into account a finite-penetration-depth excitation described in Appendix C.

The results indicate  $\mathcal{F}_{\text{th}}^{\text{SC}} = 1.4 \pm 0.4 \mu\text{J}/\text{cm}^2$  ( $R = \text{Eu}$ ) and  $0.99 \pm 0.17 \mu\text{J}/\text{cm}^2$  ( $R = \text{La}$ ) for the SC response. We note that these values are small compared to that of Bi2212

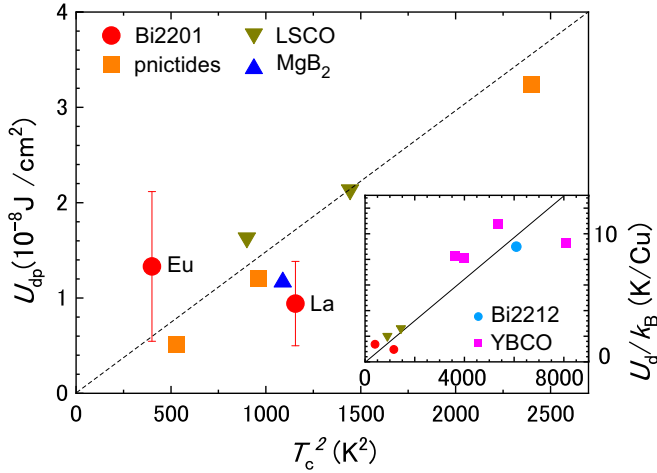


FIG. 4. The optical destruction energy planar density  $U_{dp}$  as a function of  $T_c^2$  obtained from the saturation threshold  $\mathcal{F}_{th}^{SC}$ , where Bi2201 data are compared to Fe-based pnictides,  $MgB_2$  [50] and LSCO [47]. The inset shows  $U_d$  normalized to the Cu content for various cuprates [48].

( $\mathcal{F}_{th}^{SC} = 8-14 \mu\text{J}/\text{cm}^2$  in Ref. [41,45]). By applying identical analysis to the PG response, we estimate the destruction thresholds of the PG state to be  $\mathcal{F}_{th}^{PG} = 35 \pm 8 \mu\text{J}/\text{cm}^2$  ( $R = \text{Eu}$ ) and  $25 \pm 3 \mu\text{J}/\text{cm}^2$  ( $R = \text{La}$ ).

On the other hand, the threshold for the SC destruction does not correlate with the change in  $T_c$ , and is rather higher for  $R = \text{Eu}$  than for  $R = \text{La}$ . We note that similar trend was obtained from the fits with more precise model based on Eq. (C1) with  $\mathcal{F}_{th}^{SC} = 1.75 \pm 0.36 \mu\text{J}/\text{cm}^2$  ( $R = \text{Eu}$ ) and  $1.44 \pm 0.24 \mu\text{J}/\text{cm}^2$  ( $R = \text{La}$ ). Using  $\mathcal{F}_{th}^{SC}$ , the optical energy density required to destroy the SC state in the photoexcited volume is obtained as  $U_d/k_B = \mathcal{F}_{th}^{SC}(1-r)\lambda_p = 1.4 \text{ K}/\text{Cu}$  ( $R = \text{Eu}$ ) and  $0.98 \text{ K}/\text{Cu}$  ( $R = \text{La}$ ). Here we used the optical penetration depth of  $\lambda_p = 106 \text{ nm}$  and the reflectivity of  $r = 0.16$  at the pump photon energy  $3.1 \text{ eV}$ , estimated from the La-doped OPD-Bi2201 data [51], assuming that the Eu doping does not significantly affect the relevant optical properties. These  $U_d$ s are much smaller than the energy required to thermally heat the sample above  $T_c$ , indicating a nonthermal SC destruction.

In the initial phonon-mediated carrier relaxation process, only the high-energy phonons that satisfy  $\hbar\omega > 2\Delta_{SC}$  contribute to the pair breaking, while the remaining excess energy is dissipated by the low-energy phonons.  $U_d$  is thus given by the sum of the thermodynamic condensation energy and the energy transferred to the low-energy phonons. Previous systematic measurements have shown that the latter is dominant in various high- $T_c$  superconductors [48].

In Fig. 4, we plot the single  $\text{CuO}_2$  (FeAs, Mg) plane destruction-energy planar density  $U_{dp}$  of various layered superconductors as a function of  $T_c^2$  [48,52]. The  $U_{dp}$  of La-Bi2201 follows the trend observed in Ref. [52], while the  $U_{dp}$  of Eu-Bi2201 appears anomalously large. Looking at the cuprates only (see inset of Fig. 4) and normalizing to the Cu content the La-Bi2201 data point correlates well with what was reported in Ref. [52]. The Eu-Bi2201 data point appears high also with the Cu content normalization. This indicates

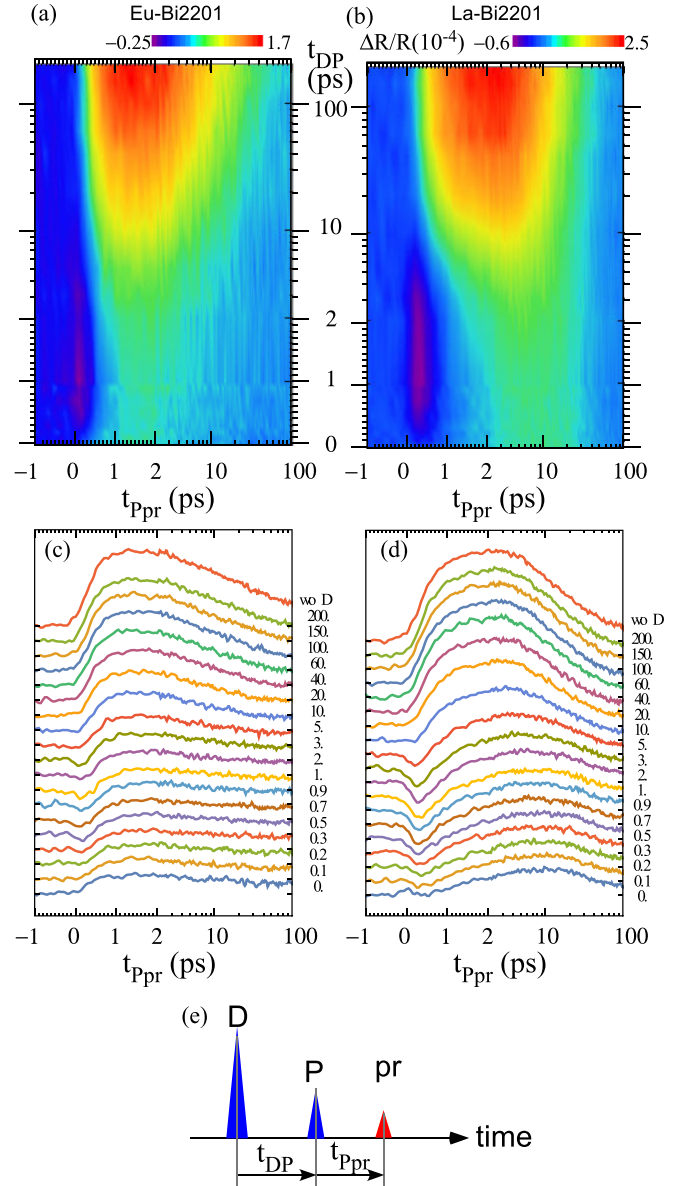


FIG. 5. Results of 3-pulse quench spectroscopy for (left) Eu-Bi2201 and (right) La-Bi2201 at  $T = 10 \text{ K}$  with the same photoexcitation conditions ( $\mathcal{F}_D = 35 \mu\text{J}/\text{cm}^2$  and  $\mathcal{F}_P = 17 \mu\text{J}/\text{cm}^2$ ). [(a), (b)] Density plots of  $\Delta r/r$  as functions of pump-probe delay time  $t_{ppr}$  and elapsed time  $t_{DP}$  after the D-pulse excitation. [(c), (d)] Transient  $\Delta r/r$  at selected  $t_{DP}$ . Each trace is vertically shifted for clarity. (e) Schematic illustration of the 3-pulse quench experiment with the delay notations.

that the assumption that the optical penetration depth is similar in both samples is incorrect with strong indication that the penetration depth in Eu-Bi2201 is significantly larger.

### C. Three-pulse quench experiments

To study the SC and PG states recovery upon photoexcitation we also employed the 3-pulse quench spectroscopy [53] combining destruction (D) pulses with the P-pr spectroscopy. Figure 5 shows the transient responses after the optical quench of Eu-Bi2201 (left) and La-Bi2201 (right) measured at

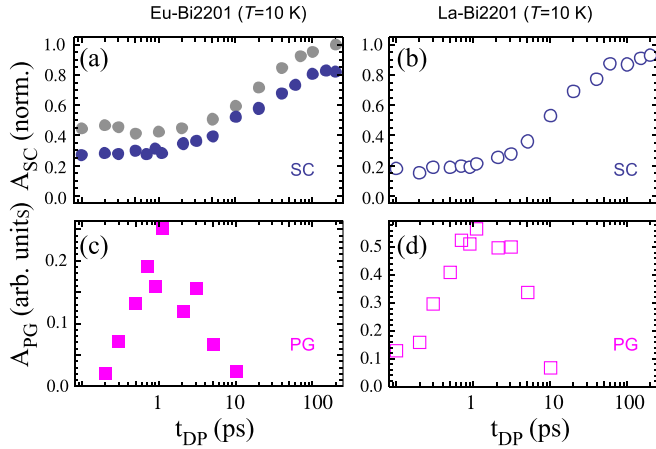


FIG. 6. Plots of [(a), (b)] SC and [(c), (d)] PG amplitudes for [(a), (c)] Eu-Bi2201 and [(b), (d)] La-Bi2201 derived from Fig. 5 ( $\mathcal{F}_D = 35 \mu\text{J}/\text{cm}^2$  and  $\mathcal{F}_P = 17 \mu\text{J}/\text{cm}^2$ ). The SC amplitudes ( $A_{SC}$ ) are normalized by the SC amplitude without the D pulse. The grey circles in (a) are the results obtained under a weaker excitation condition ( $\mathcal{F}_D = 11 \mu\text{J}/\text{cm}^2$  and  $\mathcal{F}_P = 10 \mu\text{J}/\text{cm}^2$ ).

$T = 10 \text{ K}$ , with the D-pulse fluence  $\mathcal{F}_D = 35 \mu\text{J}/\text{cm}^2$  and  $\mathcal{F}_P = 17 \mu\text{J}/\text{cm}^2$ . The  $\mathcal{F}_D$  is more than 10 times higher than the  $\mathcal{F}_{th}^{SC}$  and comparable to the  $\mathcal{F}_{th}^{PG}$ . In Figs. 5(a) and 5(b), we show the density plots of  $\Delta r/r$ , where the vertical axis corresponds to the elapsed time after the D-pulse quench  $t_{DP}$  [see Fig. 5(e) for the definition]. The  $\Delta r/r$  as a function of  $t_{DP}$  at selected  $t_{DP}$  are shown in Figs. 5(c) and 5(d). In both samples, the time regions of  $t_{DP}$ , where the SC and PG responses are dominant, are well separated, allowing comparison of the SC and PG recovery dynamics under the same optical conditions.

When the D pulse arrives, both the SC and PG components are rapidly suppressed. Then the PG component recovers first [54]. In Figs. 5(a) and 5(b)  $\Delta r/r$  up to  $t_{DP} \sim 5 \text{ ps}$  is dominated by the sub-picosecond PG response (cold-color component). Subsequently, from  $t_{DP} \sim 10 \text{ ps}$  on, the recovery of the SC response becomes dominant and changes to a response that is qualitatively similar to the  $\Delta r/r$  without the D pulse [see the top rows in Figs. 5(c) and 5(d)]. Note that  $A_{SC}$  in La-Bi2201 recovers to the same magnitude as  $A_{SC}$  without D pulse, whereas  $A_{SC}$  recovery in Eu-Bi2201 is smaller in amplitude, reaching up to 80% at the longest  $t_{DP} \sim 200 \text{ ps}$ .

The evolutions of the SC ( $A_{SC}$ ) and PG amplitudes ( $A_{PG}$ ) as a function of  $t_{DP}$  are shown in Fig. 6, where  $A_{SC}$  is normalized by the SC amplitude without the D pulse in Figs. 6(a) and 6(b). For Eu-Bi2201 we also present data obtained under a weaker quench condition ( $\mathcal{F}_D = 11 \mu\text{J}/\text{cm}^2 \sim 10\mathcal{F}_{th}^{SC}$  and  $\mathcal{F}_P = 10 \mu\text{J}/\text{cm}^2$ ). In Figs. 6(c) and 6(d), the PG starts to recover immediately after the photodestruction, and shows a peak at  $\sim 1 \text{ ps}$  reflecting the completion of the PG formation. Then  $A_{PG}$  decreases again affected by the increase in  $A_{SC}$ . A comparison of the SC and the PG recoveries indicates that the SC state grows significantly only after the completion of the PG recovery in both samples. The recovery time of the  $A_{PG}$  is  $\tau_{rec}^{PG} < 1 \text{ ps}$  for both  $R$ -Bi2201.

Due to the low  $T_c$  of Eu-Bi2201,  $A_{SC}$  is not fully recovered even at  $t_{DP} = 200 \text{ ps}$ , suggesting that the subsequent recovery is dominated by the heat diffusion from the D-pulse excitation

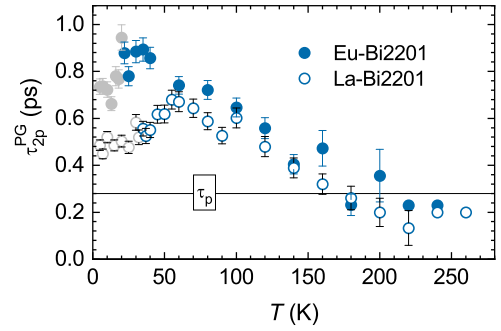


FIG. 7. The PG component relaxation time obtained by method (ii) as a function of  $T$ . The SC-state data points, where the value is affected by the the SC component risetime dynamics, are marked by different color.

volume. At the D-pulse excitation condition with the lower fluence (below  $\mathcal{F}_{th}^{PG}$ ),  $\sim 90\%$  recovery of  $A_{SC}$  is observed in Eu-Bi2201 at  $t_{DP} \approx 100 \text{ ps}$  [grey circles in Fig. 6(a)].

#### IV. DISCUSSION

First, we note that the SC dynamics of  $R$ -Bi2201 reflect the characteristics of the high- $T_c$  cuprates with small SC gap. The decay of the SC component in  $R$ -Bi2201 ( $\tau_{2p}^{SC} = 15\text{--}25 \text{ ps}$  in  $R = \text{Eu}$  and  $10\text{--}15 \text{ ps}$  in  $R = \text{La}$ ) is slower than that of Bi2212 ( $\tau_{2p}^{SC} \leq 5 \text{ ps}$ ) and close to that of LSCO ( $\tau_{2p}^{SC} \approx 10 \text{ ps}$ ). The slow SC component relaxation time is understood in the context of enhancement of the quasiparticle reexcitation by the high-energy phonons due to the small SC gap. The small optical SC destruction energy  $U_d$  in Fig. 4 is also consistent with the small SC gap.

Next, we consider the characteristics of the PG state of  $R$ -Bi2201. The relaxation time of the PG component (see Fig. 7) drops with increasing  $T$  and has similar magnitude than in other cuprates ( $\tau_{2p}^{PG} = 0.2\text{--}0.8 \text{ ps}$  for Bi2212 [41,45],  $0.2\text{--}0.6 \text{ ps}$  for LSCO [27],  $\sim 0.5 \text{ ps}$  for YBCO [55]). Consistently, in contrast to the SC dynamics,  $\tau_{2p}^{PG}$  is only weakly dependent of the  $R$  substitution in Bi2201.

Looking at the drop and the difference in (and near in La-Bi2201) the SC state it is not entirely clear whether the change can be attributed to an actual drop of  $\tau_{2p}^{PG}$  as the PG decay overlaps with the SC component rise. In Bi2212 the behavior of  $\tau^{PG}$  in the SC state is controversial since the data show no change [41] of  $\tau^{PG}$  when crossing  $T_c$  while in Y-substituted Bi2212 a drop is observed [56] below  $T_c$ . Since the Y substitution affects the out-of-plane disorder in Bi2212 and our  $R$ -Bi2201 samples show  $R$ -dependent drop there appears that the out-of-plane disorder affects the coupling between the SC and PG dynamical responses. The behavior between the two families appears anticorrelated; however, since the larger disorder ( $R = \text{Eu}$ ) sample shows a smaller relative drop of  $\tau^{PG}$ .

Because of the low  $T_c$  of Eu-Bi2201, the  $T$  dependence of the  $A_{PG}$  clearly shows a wider flat region at low- $T > T_c$ , satisfying the theoretical curve characterized by the  $T$ -independent  $\Delta_{PG}$  [Fig. 2(b) and its inset] [40]. La-Bi2201 shows a narrower flat  $A_{PG}$  region around  $T \approx 70 \text{ K}$ , which is completely absent in the direct-readout method (i) data points due to the



pronounced contribution attributed to the SC fluctuations. The enhancement of the fluctuations can also be seen directly in the SC dynamics above  $T_c$  [Fig. 2(a)] and the drop of  $\tau_{2p}^{\text{PG}}$  sets in well above  $T_c$ . The SC fluctuations therefore penetrate deeply into the PG state in La-Bi2201.

Similar to the previous ARPES and STM studies [19,20,36], our time-resolved studies suggest that the out-of-plane disorder increases the PG energy, and reduces  $T_c$ . Recent NMR studies have reported that the external pressure that promotes high  $T_c$  in cuprate superconductors redistributes holes in favor of oxygen sites [17]. On the other hand, STM studies have suggested that the charge ordering in the PG state consists of a spatially localized charge structure on oxygen sites with d-wave symmetry, and that charges on the  $O_x$  and  $O_y$  sites are modulated by the same wave vector but are out of phase [18]. Thus, the out-of-plane disorder in optimally doped samples may reduce the SC state and enhance the PG state by randomly modulating holes on oxygen sites.

Finally, we discuss the recovery dynamics of the SC and PG states. Here we note that the processes that govern the SC state recovery are essentially excitation density dependent [53,57]. Just above the destruction threshold the SC-state recovery is initiated by the fast quench of the electronic (and strongly coupled phonon) degrees of freedom to the lattice heat bath  $T$ , on a picosecond timescale, followed by the nonthermal time-dependent Ginzburg-Landau order parameter dynamics [53]. At much higher excitation densities, the lattice heat bath  $T$  exceeds  $T_c$  and the recovery is dominated by the deposited energy removal out of the excited volume on a nanosecond or slower timescale resulting in a slow quench.

In the present experiment, the maximum photoexcited lattice-bath temperature  $T_b$  near the surface at the center of the beam is estimated [58] to reach  $\sim 20$  K at  $11 \mu\text{J}/\text{cm}^2$  excitation (3-pulse low- $\mathcal{F}_D$  data, cf. Fig. 6),  $\sim 28$  K at  $35 \mu\text{J}/\text{cm}^2$  excitation (3-pulse data, cf. Fig. 5) and  $\sim 30$  K at  $45 \mu\text{J}/\text{cm}^2$  excitation (2-pulse low- $T$  data, cf. Fig. 1). The slow recovery conditions are therefore avoided in the La-Bi2201 sample at  $35 \mu\text{J}/\text{cm}^2$  excitation while in the Eu-Bi2201 sample the slow recovery conditions should be present already, due to the lower  $T_c$ . Surprisingly, both, the 2-pulse and 3-pulse data for Eu-Bi2201 do not show a clear distinction in comparison to the La-Bi2201 sample indicating that the quench conditions are similar and  $T_b$  is lower in Eu-Bi2201. As mentioned above, the optical penetration depth in Eu-Bi2201 should be therefore much larger than in La-Bi2201. Our data suggest  $\sim 2 - 3$  times larger penetration depth. Unfortunately, no optical data for Eu-Bi2201 is available to crosscheck our estimate.

Comparing the SC state recovery timescale in  $R$ -Bi2201 to LSCO [53] we find that the SC recovery in the fast-quench setting is somewhat slower in  $R$ -Bi2201 with the fast SC component recovery within  $\sim 100$  ps in comparison to  $\sim 20$  ps in LSCO. In Bi2212 [57] a much faster initial SC recovery, on a  $\sim 5$  ps timescale was observed.

Looking at the PG state suppression the behavior is very different among different cuprates. In LSCO the PG suppression threshold is very large,  $\sim 750 \mu\text{J}/\text{cm}^2$  [59] in Bi2212 is  $\sim 50 \mu\text{J}/\text{cm}^2$  [32,41] while in the present  $R$ -Bi2201 it is  $\sim 40 \mu\text{J}/\text{cm}^2$ , and does not correlate with the  $\Delta_{\text{PG}}$  magnitudes,

which are rather similar in the 30–50 meV range in LSCO, Bi2212, and  $R$ -Bi2201.

The PG state recovery was studied with the 3-pulse technique only in Bi2212 [57], where  $\tau_{\text{rec}}^{\text{PG}} = 0.6\text{--}0.8$  ps was observed at  $T > T_c$  that is nearly independent of  $F_D$  and  $T$  and is approximately equal to the 2-pulse relaxation time,  $\tau_{2p}^{\text{PG}}$ . In  $R$ -Bi2201 we observe virtually identical behavior with similar recovery times.

## V. CONCLUSIONS

In summary, we performed optical time-resolved spectroscopy on OPD  $R$ -Bi2201 with different disorders in order to investigate the SC and PG properties and their relationship to the nonequilibrium quasiparticle dynamics. Overall the observed dynamic behavior is consistent with the behavior observed in other high- $T_c$  families, where the characteristic sub-picosecond relaxation time scale in the PG state does not vary strongly among families, while the characteristic slower SC state relaxation slows down with decreasing  $T_c$ .

The difference in the spatial inhomogeneity due to the  $R$  substitution is found to affect the PG magnitude estimated from the temperature dependencies of the QP dynamics. The data also hint that the out-of-plane disorder affects the coupling between the SC and PG dynamical responses.

The presence of the SC fluctuations above  $T_c$  is observed in both samples, where especially in the La-Bi2201 sample the fluctuations appear in the temperature range more than 10 K above  $T_c$ .

The planar optical destruction energy densities of the SC state are consistent with the  $T_c^2$  dependence of the data obtained for other high- $T_c$  superconductors. The 3-pulse quench spectroscopy indicates the correlation between SC and PG in the recovery dynamics, where the SC recovery evolves cooperatively once the PG has recovered.

## ACKNOWLEDGMENTS

Y.T. and S.T. acknowledge the financial support of Japan Society for the Promotion of Science (KAKENHI Grants-in-Aid No. 19H05826, No. 22H01978). D.M. and T.M. acknowledge the financial support of Slovenian Research Agency (research core funding No-P1-0040).

## APPENDIX A: MAGNETIC SUSCEPTIBILITIES OF THE SAMPLES

The optimization of the doping level of the two samples has been checked by the optimal  $T_c^{\text{m}}$  values evaluated from the magnetic susceptibility measurements as displayed in Fig. 8.

## APPENDIX B: TEMPERATURE DEPENDENT DATA ANALYSIS AND FITS

Assuming a  $T$ -independent EPR component corresponding to the high- $T$   $\Delta r/r$  we plot in Fig. 9 the  $T$ -dependent data with subtracted EPR component,  $\Delta r_s(T) = \Delta r(T) - \Delta r(T_{\text{max}})$ , where  $T_{\text{max}} = 260$  K and  $T_{\text{max}} = 280$  K, for  $R = \text{Eu}$  and  $\text{La}$ , respectively. Similar to the case of Bi2212 [32,41], it turns out that  $\Delta r_s$  in the PG state can be described by a single exponentially relaxing component. Moreover the initial part

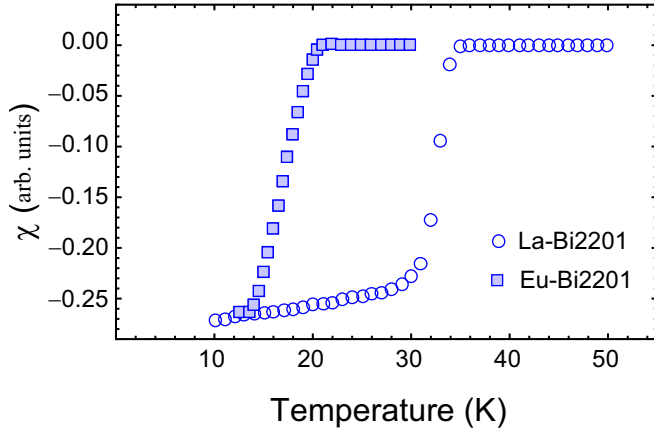


FIG. 8. Temperature dependence of magnetic susceptibility, estimated to be  $T_c^m = 34$  K for La-Bi2201 and  $T_c^m = 20$  K for Eu-Bi2201.

of the subtracted transients in the full- $T$  range can be fit by a simple two-component model,

$$\frac{\Delta r_s}{r} = A_\tau \int_0^\infty G(t-u) \exp^{-u/\tau} du + A_{\text{inf}} \int_0^\infty G(t-u) du, \quad (\text{B1})$$

where  $G(t) = \sqrt{\frac{2}{\pi}} \frac{1}{\tau_p} e^{-\frac{2t^2}{\tau_p^2}}$  corresponds to the effective excitation pulse with the characteristic width  $\tau_p$ . To fully fit the risetime we set  $\tau_p$  to be a dataset-global fit parameter and obtain  $\tau_p = 0.28 \pm 0.06$  ps, identical in both samples within the error bar. The  $\tau_p$  value is larger than the convoluted pump and probe pulse width,  $\tau_{\text{pp}} = 0.19 \pm 0.02$  ps, indicating the delayed excitation of the low energy states due to the primary photoexcited electron-hole relaxation and thermalization via electron-electron and electron-phonon scattering.

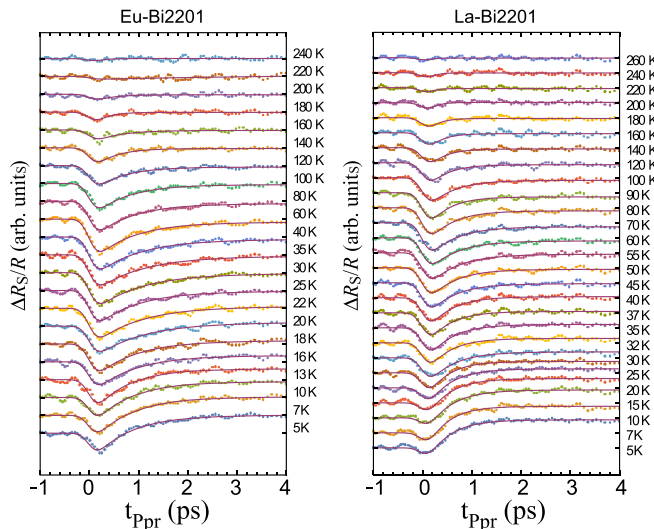


FIG. 9. Transient reflectivity with subtracted high- $T$  response. The lines are the fits discussed in text.

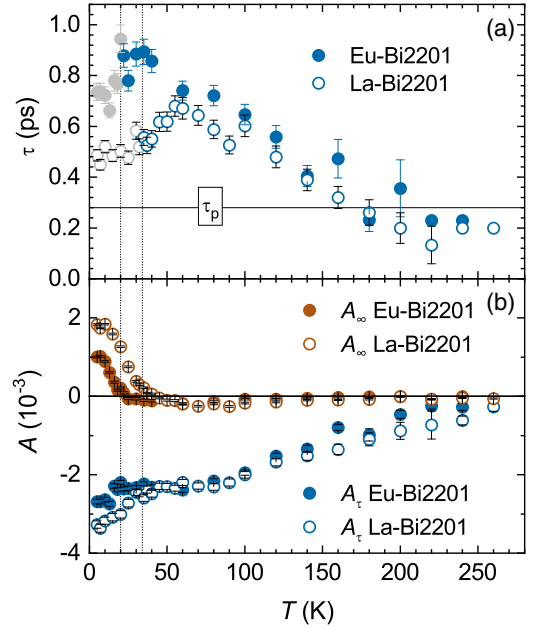


FIG. 10. Temperature dependence of the fit parameters. The vertical dotted lines correspond to the samples  $T_c$ .

In Fig. 10 we plot  $T$  dependencies of the relaxation times and component amplitudes obtained from the fit (B1). In the PG state  $A_{\text{inf}} \sim 0$  and grows when entering the SC state and can be considered a good almost-background-free proxy of the SC component amplitude  $A_{\text{SC}}$ . The fast-relaxation-component absolute amplitude  $|A_\tau|$  increases with decreasing  $T$  developing a plateau below  $T_{\text{pl}} \sim 70$  K, increasing further upon entering the SC state. The relaxation time increases with decreasing  $T$  from  $\tau \sim 0.2$  ps at the highest  $T$  showing a maximum of  $\tau \sim 0.9$  ps at  $T_m \sim 20$  K  $\sim T_c$  for  $R = \text{Eu}$  and of  $\tau \sim 0.7$  ps at  $T_m \sim 60$  K for  $R = \text{La}$  dropping to  $\tau \sim 0.7$  and  $\tau \sim 0.5$  ps in the SC state at  $T = 5$  K, for  $R = \text{Eu}$  and  $\text{La}$ , respectively. In the PG state it corresponds to the PG component amplitude,  $A_{\text{PG}} \sim |A_\tau|$ , while in the SC state an admixture of  $A_{\text{SC}}$  cannot be avoided.

### APPENDIX C: SATURATION MODEL

Assuming that the photoinduced transient dielectric function at the probe wavelength can be expressed as  $\Delta\epsilon(z) = \Delta\epsilon_0 g(z)$ , where  $g(z)$  is a real function and  $\Delta\epsilon_0$  is a complex constant, the transient reflectivity can be expressed as [60]

$$\frac{\Delta r}{r} = \frac{4\omega_{\text{pr}} |\Delta\epsilon_0|}{c_0 |\mathcal{N}^2 - 1|} \int_0^\infty dz e^{-az} \times \cos\left(2n \frac{\omega_{\text{pr}}}{c_0} z - \phi(\mathcal{N}, \Delta\epsilon_0)\right) g(z). \quad (\text{C1})$$

In addition to the probe index of refraction,  $\mathcal{N} = n + i\kappa$ , and the absorption coefficient  $\alpha(\kappa)$ , which are given by the static optical properties, the integral kernel depends on the phase shift  $\phi(\mathcal{N}, \Delta\epsilon_0)$ . The phase shift can strongly influence the kernel shape and, as a result, the depth sensitivity of the probe.



It cannot be determined from the static optical constants only and needs to be determined from the transient data.

In the case of coaxial Gaussian beams with finite diameters (C1) can be easily extended by an additional integration in the radial direction [61] where  $g(r, z)$  is obtained from an appropriate effective model by taking into account the excitation density spatial dependence,

$$U(r, z) = \mathcal{F}(1 - r_p)\alpha_p \exp\left[-\alpha_p z - \frac{2r^2}{\rho_p^2}\right], \quad (\text{C2})$$

where  $r$  corresponds to the radial distance from the beams center while  $r_p$ ,  $\alpha_p$ , and  $\rho_p$  are the pump reflectivity, absorption coefficient, and beam diameter, respectively.

To take into account the suppression of the SC (PG) state resulting in a nonlinear  $\Delta\epsilon$  excitation dependence we assume a simple phenomenological saturation model [47,60] where we approximate the local amplitude of the transient dielectric function change,  $\Delta\epsilon(r, z) \propto g(r, z)$ , by a piecewise linear function of the locally absorbed energy density  $U(r, z)$  that has different slopes below and above  $U_d$ ,

$$g(r, z) = h(U(r, z)),$$

$$h(u) = \begin{cases} \frac{u}{U_d}; & u < U_{th} \\ 1 + a\left(\frac{u}{U_d} - 1\right); & u \geq U_{th} \end{cases}. \quad (\text{C3})$$

Here  $a$  corresponds to the relative slope in the normal state, while  $U_d$  is related to the external threshold fluence by  $U_d = \mathcal{F}_{th}(1 - r_p)\alpha_p$ .

In the literature [41,47,48,52] by some of the present authors, simplified less-accurate kernel with omitted  $\cos(\dots)$  factor was used. In order to compare with the previous results (see Fig. 4) we therefore use Eq. (C1) with the  $\cos(\dots)$  factor omitted while reporting also the more accurate values separately.

#### APPENDIX D: ERROR BARS OF THE OPTICAL DESTRUCTION ENERGY PLANAR DENSITY $U_{dp}$

The error bars on  $U_{dp}$  include two contributions. Apart from the statistical fitting error there is a systematic error of the optical penetration depth, which was approximated from a similar optimally doped La-(Bi,Pb)2201 sample in Heumen *et al.* [51]. Such error cannot be reliably estimated. For the La-Bi2201 sample, which is the most similar to La-(Bi,Pb)2201, the spread of data with varying the doping and Pb content in Heumen *et al.* suggests an optical conductivity error of  $\sim 30\%$  at the pump-photon energy. For the (less similar) Eu-Bi2201 sample the error must be even larger. As discussed in the main text, the highest fluence 3-pulsed data for this sample indicate that the optical-conductivity estimate systematic error must be in the  $\sim 60\%$  range.

- 
- [1] T. Timusk and B. Statt, The pseudogap in high-temperature superconductors: An experimental survey, *Rep. Prog. Phys.* **62**, 61 (1999).
- [2] K. Tanaka, W. Lee, D. Lu, A. Fujimori, T. Fujii, I. Terasaki, D. Scalapino, T. Devereaux, Z. Hussain, Z.-X. Shen *et al.*, Distinct fermi-momentum-dependent energy gaps in deeply underdoped Bi2212, *Science* **314**, 1910 (2006).
- [3] T. Kondo, T. Takeuchi, A. Kaminski, S. Tsuda, and S. Shin, Evidence for two energy scales in the superconducting state of optimally doped (Bi, Pb)<sub>2</sub>(Sr, La)<sub>2</sub>CuO<sub>6+ $\delta$</sub> , *Phys. Rev. Lett.* **98**, 267004 (2007).
- [4] M. Hashimoto, I. M. Vishik, R.-H. He, T. P. Devereaux, and Z.-X. Shen, Energy gaps in high-transition-temperature cuprate superconductors, *Nat. Phys.* **10**, 483 (2014).
- [5] H. Kontani, Y. Yamakawa, R. Tazai, and S. Onari, Odd-parity spin-loop-current order mediated by transverse spin fluctuations in cuprates and related electron systems, *Phys. Rev. Res.* **3**, 013127 (2021).
- [6] C. V. Parker, P. Aynajian, E. H. da Silva Neto, A. Pushp, S. Ono, J. Wen, Z. Xu, G. Gu, and A. Yazdani, Fluctuating stripes at the onset of the pseudogap in the high- $T_c$  superconductor Bi<sub>2</sub>Sr<sub>2</sub>CaCu<sub>2</sub>O<sub>8+x</sub>, *Nature (London)* **468**, 677 (2010).
- [7] Y. Kohsaka, C. Taylor, K. Fujita, A. Schmidt, C. Lupien, T. Hanaguri, M. Azuma, M. Takano, H. Eisaki, H. Takagi *et al.*, An intrinsic bond-centered electronic glass with unidirectional domains in underdoped cuprates, *Science* **315**, 1380 (2007).
- [8] X. Li, C. Zou, Y. Ding, H. Yan, S. Ye, H. Li, Z. Hao, L. Zhao, X. Zhou, and Y. Wang, Evolution of charge and pair density modulations in overdoped Bi<sub>2</sub>Sr<sub>2</sub>CuO<sub>6+ $\delta$</sub> , *Phys. Rev. X* **11**, 011007 (2021).
- [9] Y. Sato, S. Kasahara, H. Murayama, Y. Kasahara, E.-G. Moon, T. Nishizaki, T. Loew, J. Porras, B. Keimer, T. Shibauchi *et al.*, Thermodynamic evidence for a nematic phase transition at the onset of the pseudogap in YBa<sub>2</sub>Cu<sub>3</sub>O<sub>y</sub>, *Nat. Phys.* **13**, 1074 (2017).
- [10] L. Mangin-Thro, Y. Sidis, A. Wildes, and P. Bourges, Intra-unit-cell magnetic correlations near optimal doping in YBa<sub>2</sub>Cu<sub>3</sub>O<sub>6.85</sub>, *Nat. Commun.* **6**, 7705 (2015).
- [11] J. Attfield, A. Kharlanov, and J. McAllister, Cation effects in doped La<sub>2</sub>CuO<sub>4</sub> superconductors, *Nature (London)* **394**, 157 (1998).
- [12] H. Eisaki, N. Kaneko, D. L. Feng, A. Damascelli, P. K. Mang, K. M. Shen, Z.-X. Shen, and M. Greven, Effect of chemical inhomogeneity in bismuth-based copper oxide superconductors, *Phys. Rev. B* **69**, 064512 (2004).
- [13] K. Fujita, T. Noda, K. M. Kojima, H. Eisaki, and S. Uchida, Effect of disorder outside the CuO<sub>2</sub> planes on  $T_c$  of copper oxide superconductors, *Phys. Rev. Lett.* **95**, 097006 (2005).
- [14] M. Hashimoto, T. Yoshida, A. Fujimori, D. H. Lu, Z.-X. Shen, M. Kubota, K. Ono, M. Ishikado, K. Fujita, and S. Uchida, Effects of out-of-plane disorder on the nodal quasiparticle and superconducting gap in single-layer Bi<sub>2</sub>Sr<sub>1.6</sub>La<sub>0.4</sub>CuO<sub>6+ $\delta$</sub>  ( $L = \text{La, Nd, Gd}$ ), *Phys. Rev. B* **79**, 144517 (2009).
- [15] H. Hobou, S. Ishida, K. Fujita, M. Ishikado, K. M. Kojima, H. Eisaki, and S. Uchida, Enhancement of the superconducting critical temperature in Bi<sub>2</sub>Sr<sub>2</sub>CaCu<sub>2</sub>O<sub>8+ $\delta$</sub>  by controlling disorder outside CuO<sub>2</sub> planes, *Phys. Rev. B* **79**, 064507 (2009).
- [16] K. Kurokawa, S. Isono, Y. Kohama, S. Kunisada, S. Sakai, R. Sekine, M. Okubo, M. D. Watson, T. K. Kim, C. Cacho *et al.*, Unveiling phase diagram of the lightly doped high- $T_c$

- cuprate superconductors with disorder removed, *Nat. Commun.* **14**, 4064 (2023).
- [17] M. Jurkutat, C. Kattinger, S. Tsankov, R. Reznicek, A. Erb, and J. Haase, How pressure enhances the critical temperature of superconductivity in  $\text{YBa}_2\text{Cu}_3\text{O}_{6+y}$ , *Proc. Natl. Acad. Sci. USA* **120**, e2215458120 (2023).
- [18] K. Fujita, M. H. Hamidian, S. D. Edkins, C. K. Kim, Y. Kohsaka, M. Azuma, M. Takano, H. Takagi, H. Eisaki, S.-i. Uchida *et al.*, Direct phase-sensitive identification of ad-form factor density wave in underdoped cuprates, *Proc. Natl. Acad. Sci. USA* **111**, E3026 (2014).
- [19] Y. Okada, T. Takeuchi, A. Shimoyamada, S. Shin, and H. Ikuta, The influence of out-of-plane disorder on the formation of pseudogap and fermi arc in  $\text{Bi}_2\text{Sr}_{2-x}\text{R}_x\text{CuO}_y$  ( $\text{R} = \text{La}$  and  $\text{Eu}$ ), *J. Phys. Chem. Solids* **69**, 2989 (2008).
- [20] Y. Okada, T. Kawaguchi, M. Ohkawa, K. Ishizaka, T. Takeuchi, S. Shin, and H. Ikuta, Three energy scales characterizing the competing pseudogap state, the incoherent, and the coherent superconducting state in high- $T_c$  cuprates, *Phys. Rev. B* **83**, 104502 (2011).
- [21] J. Demsar, Non-equilibrium phenomena in superconductors probed by femtosecond time-domain spectroscopy, *J. Low Temp. Phys.* **201**, 676 (2020).
- [22] C. Giannetti, F. Cilento, S. Dal Conte, G. Coslovich, G. Ferrini, H. Molegraaf, M. Raichle, R. Liang, H. Eisaki, M. Greven *et al.*, Revealing the high-energy electronic excitations underlying the onset of high-temperature superconductivity in cuprates, *Nat. Commun.* **2**, 353 (2011).
- [23] F. Giusti, A. Marciniak, F. Randi, G. Sparapassi, F. Boschini, H. Eisaki, M. Greven, A. Damascelli, A. Avella, and D. Fausti, Signatures of enhanced superconducting phase coherence in optimally doped  $\text{Bi}_2\text{Sr}_2\text{Y}_{0.08}\text{Ca}_{0.92}\text{Cu}_2\text{O}_{8+\delta}$  driven by midinfrared pulse excitations, *Phys. Rev. Lett.* **122**, 067002 (2019).
- [24] J. Demsar, R. Hudej, J. Karpinski, V. V. Kabanov, and D. Mihailovic, Quasiparticle dynamics and gap structure in  $\text{HgBa}_2\text{Ca}_2\text{Cu}_3\text{O}_{8+\delta}$  investigated with femtosecond spectroscopy, *Phys. Rev. B* **63**, 054519 (2001).
- [25] D. Dvorsek, V. V. Kabanov, J. Demsar, S. M. Kazakov, J. Karpinski, and D. Mihailovic, Femtosecond quasiparticle relaxation dynamics and probe polarization anisotropy in  $\text{YSr}_x\text{Ba}_{2-x}\text{Cu}_4\text{O}_8$  ( $x = 0, 0.4$ ), *Phys. Rev. B* **66**, 020510(R) (2002).
- [26] G. P. Segre, N. Gedik, J. Orenstein, D. A. Bonn, R. Liang, and W. N. Hardy, Photoinduced changes of reflectivity in single crystals of  $\text{YBa}_2\text{Cu}_3\text{O}_{6.5}$  (ortho II), *Phys. Rev. Lett.* **88**, 137001 (2002).
- [27] P. Kusar, J. Demsar, D. Mihailovic, and S. Sugai, A systematic study of femtosecond quasiparticle relaxation processes in  $\text{La}_{2-x}\text{Sr}_x\text{CuO}_4$ , *Phys. Rev. B* **72**, 014544 (2005).
- [28] Y. H. Liu, Y. Toda, K. Shimatake, N. Momono, M. Oda, and M. Ido, Direct observation of the coexistence of the pseudogap and superconducting quasiparticles in  $\text{Bi}_2\text{Sr}_2\text{CaCu}_2\text{O}_{8+y}$  by time-resolved optical spectroscopy, *Phys. Rev. Lett.* **101**, 137003 (2008).
- [29] C. W. Luo, H. P. Lo, C. H. Su, I. H. Wu, Y.-J. Chen, K. H. Wu, J.-Y. Lin, T. M. Uen, J. Y. Juang, and T. Kobayashi, Doping dependence of the ultrafast electronic dynamics of  $\text{Y}_{1-x}\text{Pr}_x\text{Ba}_2\text{Cu}_3\text{O}_{7-\delta}$  thin-film superconductors from femtosecond optical spectroscopy, *Phys. Rev. B* **82**, 104512 (2010).
- [30] Y. Toda, F. Kawanokami, T. Kurosawa, M. Oda, I. Madan, T. Mertelj, V. V. Kabanov, and D. Mihailovic, Rotational symmetry breaking in  $\text{Bi}_2\text{Sr}_2\text{CaCu}_2\text{O}_{8+\delta}$  probed by polarized femtosecond spectroscopy, *Phys. Rev. B* **90**, 094513 (2014).
- [31] F. Giusti, A. Montanaro, A. Marciniak, F. Randi, F. Boschini, F. Glerean, G. Jarc, H. Eisaki, M. Greven, A. Damascelli, A. Avella, and D. Fausti, Anisotropic time-domain electronic response in cuprates driven by midinfrared pulses, *Phys. Rev. B* **104**, 125121 (2021).
- [32] I. Madan, T. Kurosawa, Y. Toda, M. Oda, T. Mertelj, and D. Mihailovic, Evidence for carrier localization in the pseudogap state of cuprate superconductors from coherent quench experiments, *Nat. Commun.* **6**, 6958 (2015).
- [33] S. Peli, S. D. Conte, R. Comin, N. Nembrini, A. Ronchi, P. Abrami, F. Banfi, G. Ferrini, D. Brida, S. Lupi *et al.*, Mottness at finite doping and charge instabilities in cuprates, *Nat. Phys.* **13**, 806 (2017).
- [34] S. Dal Conte, L. Vidmar, D. Golež, M. Mierzejewski, G. Soavi, S. Peli, F. Banfi, G. Ferrini, R. Comin, B. M. Ludbrook *et al.*, Snapshots of the retarded interaction of charge carriers with ultrafast fluctuations in cuprates, *Nat. Phys.* **11**, 421 (2015).
- [35] A. Sugimoto, S. Kashiwaya, H. Eisaki, H. Kashiwaya, H. Tsuchiura, Y. Tanaka, K. Fujita, and S. Uchida, Enhancement of electronic inhomogeneities due to out-of-plane disorder in  $\text{Bi}_2\text{Sr}_2\text{CuO}_{6+\delta}$  superconductors observed by scanning tunneling spectroscopy, *Phys. Rev. B* **74**, 094503 (2006).
- [36] T. Kurosawa, K. Takeyama, S. Baar, Y. Shibata, M. Kataoka, S. Mizuta, H. Yoshida, N. Momono, M. Oda, and M. Ido, Out-of-plane disorder effects on the energy gaps and electronic charge order in  $\text{Bi}_2\text{Sr}_{1.7}\text{R}_{0.3}\text{CuO}_{6+\delta}$  ( $\text{R} = \text{La}$  and  $\text{Eu}$ ), *J. Phys. Soc. Jpn.* **85**, 044709 (2016).
- [37] T. Mertelj, P. Kusar, V. V. Kabanov, L. Stojchevska, N. D. Zhigadlo, S. Katrych, Z. Bukowski, J. Karpinski, S. Weyeneth, and D. Mihailovic, Quasiparticle relaxation dynamics in spin-density-wave and superconducting  $\text{SmFeAsO}_{1-x}\text{F}_x$  single crystals, *Phys. Rev. B* **81**, 224504 (2010).
- [38] I. Madan, T. Kurosawa, Y. Toda, M. Oda, T. Mertelj, P. Kusar, and D. Mihailovic, Separating pairing from quantum phase coherence dynamics above the superconducting transition by femtosecond spectroscopy, *Sci. Rep.* **4**, 5656 (2014).
- [39] T. Mertelj, V. V. Kabanov, C. Gadermaier, N. D. Zhigadlo, S. Katrych, J. Karpinski, and D. Mihailovic, Distinct pseudogap and quasiparticle relaxation dynamics in the superconducting state of nearly optimally doped  $\text{SmFeAsO}_{0.8}\text{F}_{0.2}$  single crystals, *Phys. Rev. Lett.* **102**, 117002 (2009).
- [40] V. V. Kabanov, J. Demsar, B. Podobnik, and D. Mihailovic, Quasiparticle relaxation dynamics in superconductors with different gap structures: Theory and experiments on  $\text{YBa}_2\text{Cu}_3\text{O}_{7-\delta}$ , *Phys. Rev. B* **59**, 1497 (1999).
- [41] Y. Toda, T. Mertelj, P. Kusar, T. Kurosawa, M. Oda, M. Ido, and D. Mihailovic, Quasiparticle relaxation dynamics in underdoped  $\text{Bi}_2\text{Sr}_2\text{CaCu}_2\text{O}_{8+\delta}$  by two-color pump-probe spectroscopy, *Phys. Rev. B* **84**, 174516 (2011).
- [42] Upon photoexcitation the initial high-energy electron-hole quasiparticles in metals relax by Auger processes as well as by phonon emission forming a rather universal transient quasiparticle energy distribution function [62] (TQEDF). The transient reflectivity change due to the TQEDF can be represented by some weighted integral over energy. The weight function (WF)

- depends on the electronic structure details. In the case when the high energy part of the TQEDF is dominating the normal-state transient reflectivity it is plausible that the temperature dependence of this component should be weak since the appearance of the PG and the SC gap mostly affects the lower-energy parts of the WF and TQEDF, which do not contribute significantly to the response in the normal state.
- [43] For method (i)  $A_{PG}$  was estimated at  $t_{ppr} = 0.3$  ps, where  $\Delta r/r$  shows a minimum at the temperatures where the PG state develops well. The negative offset of  $A_{PG}$  in the high-temperature region is due to the fast relaxation component of the EPR response, which is assumed to be constant throughout all temperatures, while the drop in the SC state is due to the presence of the SC component for the  $R = \text{Eu}$  and  $R = \text{La}$  samples, respectively.
- [44] The values in parentheses correspond to method (i).
- [45] Y. Toda, S. Tsuchiya, M. Oda, T. Kurosawa, S. Katsumata, M. Naseska, T. Mertelj, and D. Mihailovic, Ultrafast transient reflectivity measurements of optimally doped  $\text{Bi}_{2+x}\text{Sr}_{2-x}\text{CaCu}_2\text{O}_{8+\delta}$  with disorder, *Phys. Rev. B* **104**, 094507 (2021).
- [46] The high- $T$  measurements indicate a linear scaling of the EPR response with increasing fluence. However, method (ii) is very demanding experimentally since it would require high- $T$  fluence dependence measurements of the EPR component at identical conditions.
- [47] P. Kusar, V. V. Kabanov, S. Sugai, J. Demsar, T. Mertelj, and D. Mihailovic, Controlled vaporization of the superconducting condensate in cuprate superconductors by femtosecond photoexcitation, *Phys. Rev. Lett.* **101**, 227001 (2008).
- [48] L. Stojchevska, P. Kusar, T. Mertelj, V. V. Kabanov, Y. Toda, X. Yao, and D. Mihailovic, Mechanisms of nonthermal destruction of the superconducting state and melting of the charge-density-wave state by femtosecond laser pulses, *Phys. Rev. B* **84**, 180507(R) (2011).
- [49] The weak fluence corresponds to the linear F-scaling region.
- [50] J. Demsar, R. D. Averitt, A. J. Taylor, W.-N. Kang, H. J. Kim, E.-M. Choi, and S.-I. Lee, Photoinduced conductivity dynamics studies of  $\text{MgB}_2$  thin films, *Int. J. Mod. Phys. B* **17**, 3675 (2003).
- [51] E. van Heumen, W. Meevasana, A. Kuzmenko, H. Eisaki, and D. Van Der Marel, Doping-dependent optical properties of  $\text{Bi2201}$ , *New J. Phys.* **11**, 055067 (2009).
- [52] A. Pogrebna, T. Mertelj, Z. R. Ye, D. L. Feng, and D. Mihailovic, Superconducting gap in  $\text{BaFe}_2(\text{As}_{1-x}\text{P}_x)_2$  from temperature-dependent transient optical reflectivity, *Phys. Rev. B* **92**, 144503 (2015).
- [53] I. Madan, P. Kusar, V. V. Kabanov, M. Lu-Dac, V. V. Kabanov, T. Mertelj, and D. Mihailovic, Real-time measurement of the emergence of superconducting order in a high-temperature superconductor, *Phys. Rev. B* **93**, 224520 (2016).
- [54] Contrary to  $\text{Bi2212}$  [32] the EPR does not appear clearly at short  $t_{DP}$  as well as at high  $\mathcal{F}_p$  in Fig. (3). The reason is a rather large mismatch of the pump,  $\alpha_p^{-1} \approx 106$  nm, and the probe,  $\alpha_{pr}^{-1} \approx 270$  nm, penetration depths and small  $\frac{\mathcal{F}_p}{\mathcal{F}_{th}} \sim 3$  ratio. Due to this the residual PG response from the deeper unsuppressed excited volume region is comparable to the EPR response and masks it.
- [55] J. Demsar, B. Podobnik, V. V. Kabanov, T. Wolf, and D. Mihailovic, Superconducting gap  $\Delta_c$ , the pseudogap  $\Delta_p$ , and pair fluctuations above  $T_c$  in overdoped  $\text{Y}_{1-x}\text{Ca}_x\text{Ba}_2\text{Cu}_3\text{O}_{7-\delta}$  from femtosecond time-domain spectroscopy, *Phys. Rev. Lett.* **82**, 4918 (1999).
- [56] G. Coslovich, C. Giannetti, F. Cilento, S. Dal Conte, T. Abebaw, D. Bossini, G. Ferrini, H. Eisaki, M. Greven, A. Damascelli, and F. Parmigiani, Competition between the pseudogap and superconducting states of  $\text{Bi}_2\text{Sr}_2\text{Ca}_{0.92}\text{Y}_{0.08}\text{Cu}_2\text{O}_{8+\delta}$  single crystals revealed by ultrafast broadband optical reflectivity, *Phys. Rev. Lett.* **110**, 107003 (2013).
- [57] I. Madan, V. V. Kabanov, Y. Toda, M. Oda, T. Kurosawa, V. V. Kabanov, T. Mertelj, and D. Mihailovic, Dynamics of superconducting order parameter through ultrafast normal-to-superconducting phase transition in  $\text{Bi}_2\text{Sr}_2\text{CaCu}_2\text{O}_{8+\delta}$  from multipulse polarization-resolved transient optical reflectivity, *Phys. Rev. B* **96**, 184522 (2017).
- [58] We used the heat capacity data from [63] and optical data (La doped) from Van Heumen *et al.* [51].
- [59] P. Kušar, V. V. Kabanov, S. Sugai, J. Demšar, T. Mertelj, and D. Mihailović, Dynamical structural instabilities in  $\text{La}_{1.9}\text{Sr}_{0.1}\text{CuO}_4$  under intense laser photoexcitation, *J. Supercond. Novel Magn.* **24**, 421 (2011).
- [60] M. Naseska, A. Pogrebna, G. Cao, Z. A. Xu, D. Mihailovic, and T. Mertelj, Ultrafast destruction and recovery of the spin density wave order in iron-based pnictides: A multipulse optical study, *Phys. Rev. B* **98**, 035148 (2018).
- [61] When both diameters are much larger than the corresponding wavelengths.
- [62] V. V. Kabanov and V. V. Kabanov, Theory of electronic relaxation in a metal excited by an ultrashort optical pump, *Phys. Rev. B* **89**, 125102 (2014).
- [63] A. Amoretti, M. Meinero, D. K. Brattan, F. Caglieris, E. Giannini, M. Affronte, C. Hess, B. Buechner, N. Magnoli, and M. Putti, Hydrodynamical description for magneto-transport in the strange metal phase of  $\text{Bi-2201}$ , *Phys. Rev. Res.* **2**, 023387 (2020).